Synergistic effect of nanosheet array-like NiFe-LDH and reduced graphene oxide modified Ni foam for greatly enhanced oxygen evolution reaction and hydrogen evolution reaction

Kun Wang, Jiawei Guo, Hui Zhang*

State Key Laboratory of Chemical Resource Engineering, Beijing University of Chemical Technology, Beijing 100029, China.

*Correspondence should be addressed to Hui Zhang.

E-mail: zhanghui@buct.edu.cn, huizhang67@gst21.com

Tel.: +8610 64425872;

Fax: +8610 64425385;

Number of pages: **22**

Number of figures: **9**

Number of tables: **7**

Table of Contents

Experimental

1. Chemicals and materials

Natural graphite powder (325 mesh, >99.5%) was bought from Qingdao Huatai Lubrication and Sealing Technology Co., Ltd. $Ni(NO_3)_2·6H_2O$, $Fe(NO_3)_2·9H_2O$, RuO_2 and 20% Pt/C were obtained from Aladdin. Citric acid ($C_6H_8O_7•6H_2O$) was purchased from Beijing Chemical Works (China). Acetone (C_3H_6O, ≥99.9%) and Ethanol (C_2H_5OH, ≥99.9%) were purchased from Thermo Fisher Scientific, and nickel foam was purchased from Saibo Company. All reagents can be used without further purification. Throughout the experiment, the resistivity of the deionized water was greater than 18.25 MΩ cm (25 °C).

2. Synthesis

2.1 Synthesis of rGO/NF

Using natural flake graphite as raw material, the modified Hummers method is used to prepare GO sol[1] and the details followed our precious work[2-4]. 5.37 mL (60 mg) GO sol (concentration: 11.16 mg/mL, V = 60/11.16 = 5.37 mL, excess) was placed in 60 mL deionized water, ultrasonicated for 20 min, and then 30 mg of citric acid (CA) was added for further ultrasonication for 10 min to obtain the CA-GO suspension. The obtained CA-GO suspension was placed into a 100 mL autoclave with two pieces of clean nickel foam (abbreviated as NF, 95% purity, cut to 3 cm × 5 cm size, then ultrasonically clean NF with acetone and 3 mol L^{-1} concentrated HCl for 15 min to remove oxides on the surface, followed by ultrasonically cleaning with deionized water until the pH～7, then continue ultrasonically cleaning with anhydrous ethanol for 5 min to ensure that the NF surface is well cleaned, and finally vacuum dried at 80°C for 2 h) jammed into the autoclave with a longer edge of 5 cm and sealed, kept

at 120°C for 5 h. Until the autoclave cooled off naturally, followed repeatedly rinsed with deionized water to wash away the rGO attached on the surface and the pores of the NF skeleton, and freeze-dried to obtain rGO/NF.

2.2 Synthesis of Ni_xFe_1-LDH/rGO/NF (x=3, 2, 1) composites

NiFe-LDH were prepared on rGO/NF by a simple green hydrothermal method. 0.29 g $Ni(NO_3)_2 \cdot 6H_2O$ (1 mmol), 0.4 g $Fe(NO_3)_3 \cdot 9H_2O$ (1 mmol) and 0.6 g $CO(NH_2)_2$ (10 mmol) were dissolved in 80 mL deionized water to form a clear solution (Ni:Fe = 1:1). Then the above solution was transferred to a 100 mL autoclave with a piece of as-prepared rGO/NF tilted on the inner wall of the autoclave and sealed. It was kept at 120°C for 12 h, and naturally cooled to room temperature after the reaction. Subsequently, the composites were washed with distilled water and ethanol by sonication for 5 min and vacuum freeze-drying for 6 h, the obtained composite was named as Ni_1Fe_1-LDH/rGO/NF. Ni_3Fe_1-LDH/rGO/NF, Ni_2Fe_1-LDH/rGO/NF, control samples of Ni_2Fe_1-LDH/NF and Ni_2Fe_1-LDH were prepared by the similar method without changing the total content (2 mmol).

2.3 Preparation of RuO_2 and 20% Pt/C electrodes.

RuO_2 (50 mg) was dispersed in a 1 mL mixed solution (770 μL water, 30 μL 5 wt % Nafion solution, and 200 μL ethanol), followed by sonication to obtain a catalyst ink. The catalyst ink (113 μL) was then dropcast on the surface of Ni foam (1 cm × 1 cm), which was dried at 80°C for 4 h. Pt/C electrode were prepared in a similar fashion. The catalyst loading was all ca. 5.0 mg cm^{-2}.

3. Material Characterization

The X-ray diffraction (XRD) patterns were recorded on the Shimadzu XRD-6000 diffractometer with Cu-Kα radiation (λ=0.15418 nm, 30 mA, 40 kV) as the source in the 2θ scanning range of 3-80°, at a scanning speed of 10°/min. The morphology of the samples was analyzed by scanning electron microscope (SEM) on Hitachi S-3500N operating at 20 kV. Transmission electron microscope (HRTEM) images were obtained on JEM 2010 instrument operating at 200 kV. The Raman spectra were obtained with a Jobin Yvon Hodiba Raman spectrometer model HR800 using a 532 nm line of Ar^+ ion laser as the excitation source at room temperature. X-ray photoelectron spectroscopy (XPS) results was recorded on the Vgescalab-250 (Al Ka radiator). The content of metal components was determined by inductively coupled plasma (ICP) emission spectroscopy on a Shimadzu ICPS-7500 instrument.

4. Electrochemical characterization

The electrochemical experiments involved in this study were carried out at room temperature using CHI660D electrochemical workstation (ChenHua Instruments, Shanghai, China) in 1M KOH aqueous solution as electrolyte. OER and HER measurements were conducted in the three electrodes. Using the as-prepared catalysts, the saturated Hg/HgO electrode as the working electrode (the submerged area is 1×1 cm^{-2}) and reference electrode, respectively. The counter electrode of OER and HER are the platinum plate (the area is 1×1 cm^{-2}) and graphite rod (to eliminate the influence of platinum plate on HER), respectively. A two-electrode cell was used on the same workstation for overall water splitting test, in which the electrocatalyst was directly used as anode and cathode at the same time. And the electrolyte

must be degassed by bubbling N_2 for at least 20 min before all the electrochemical experiments. We activated the electrocatalysts with 50 mV s^{-1} through CV (from 0 to 0.8 V versus saturated Hg/HgO in OER, from -0.8 to -1.9 versus saturated Hg/HgO in HER) cycles until it reached a steady state after 40 cycles. According to the Nernst equation (Eq. (S1)), all the measured potentials of electrocatalysts were converted to a reversible hydrogen electrode (RHE).

$$E_{RHE} = E_{Hg\,/\,HgO} + 0.098 + 0.0592 \times pH \quad (S1)$$

The electrocatalytic activity of all the catalysts were measured using liner sweep voltammetry (LSV) at 5 mV s^{-1}. And all the polarization curves acquired were corrected with 90% iR compensation (i and R are the test current and compensation resistance between the reference electrode and the working electrode, respectively). The overpotentials (η) were obtained by the equation (Eq. (S2)):

$$\eta = E_{vs.RHE} - 1.23 \quad (S2)$$

Derived the Tafel slopes according to the polarization curve and fitted according to the Tafel equation (Eq. (S3)):

$$\eta = a + b \log j \quad (S3)$$

where a represents a constant, b represents the Tafel slope, and j represents the measured current density. The double-layer capacitance (C_{dl}) was evaluated by cyclic voltammetry (CV) in 0.2-0.3 V versus saturated Hg/HgO electrode at scanning rates of 10, 20, 30, 40 and 50 mV s^{-1}, respectively. The long-term stability of electrocatalysts were evaluated through the chronoamperometry measurement. Electrochemical impedance spectroscopy (EIS) of 10 kHz to 0.01 Hz was measured at an applied voltage of 10 mV.

The TOF values of the Ni_2Fe_1-LDH/rGO/NF as OER and HER catalysts was calculated

according to the equations (Eq. (S4) and Eq. (S5)):

$$\text{For OER: TOF} = \frac{J \times A}{4 \times F \times m} \quad \text{(S4)}$$

$$\text{For HER: TOF} = \frac{J \times A}{2 \times F \times m} \quad \text{(S5)}$$

where j is the current density at overpotential of 0.3 V in A cm^{-2}, A is surface area of the working electrode (1 cm^2), F is the faraday constant (a value of 96485 C mol^{-1}) and m is concentration of active sites in the catalyst (mol cm^{-2}).

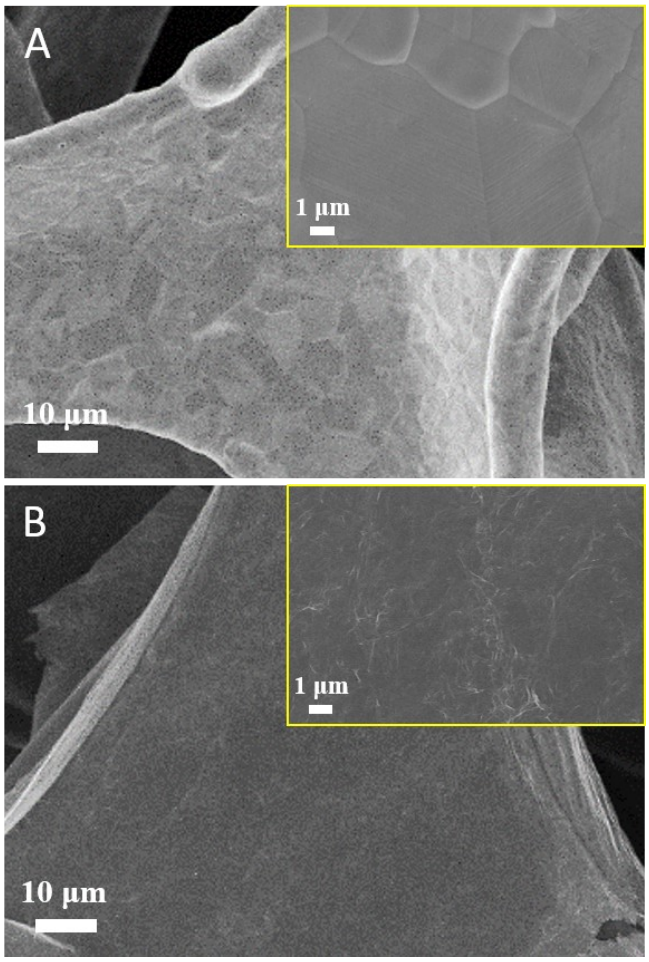

Fig. S1 SEM images of (A) NF and (B) rGO/NF.

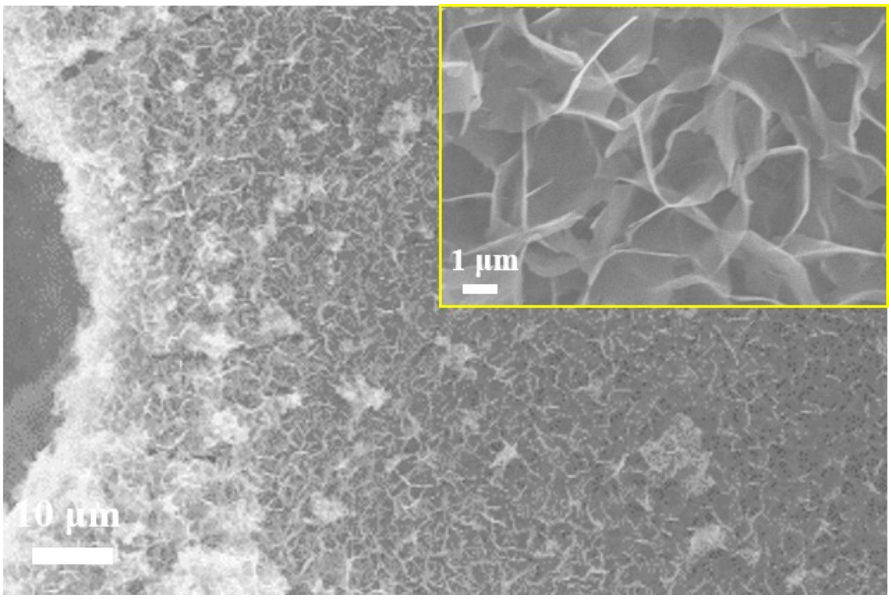

Fig. S2 SEM image of Ni_2Fe_1-LDH/NF.

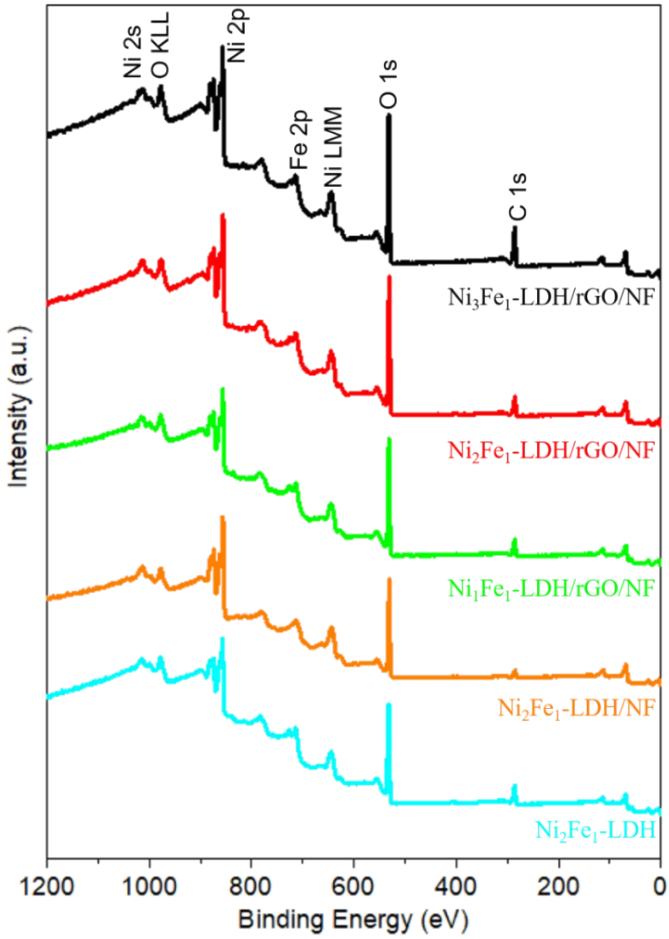

Fig. S3 Full XPS survey spectrums of Ni_xFe_1-LDH/rGO/NF (x=3, 2, 1), Ni_2Fe_1-LDH/NF and Ni_2Fe_1-LDH.

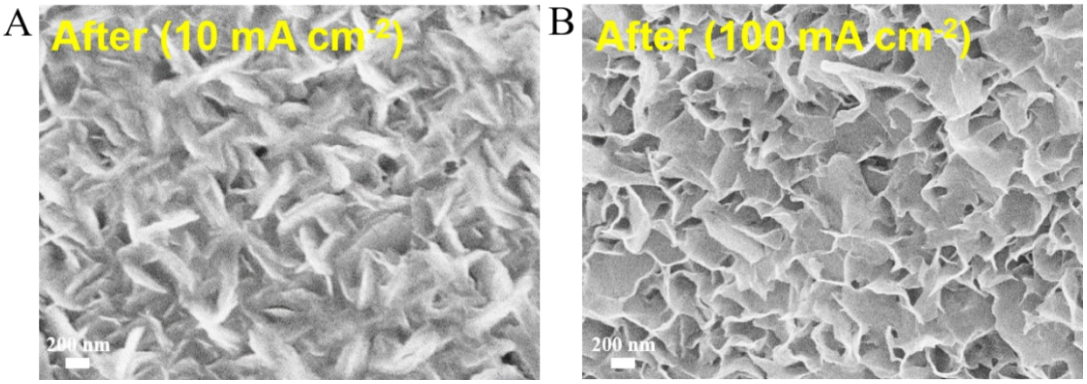

Fig. S4 (A, B) SEM images of Ni_2Fe_1-LDH/rGO/NF after the 24 h OER chronoamperometry measurement.

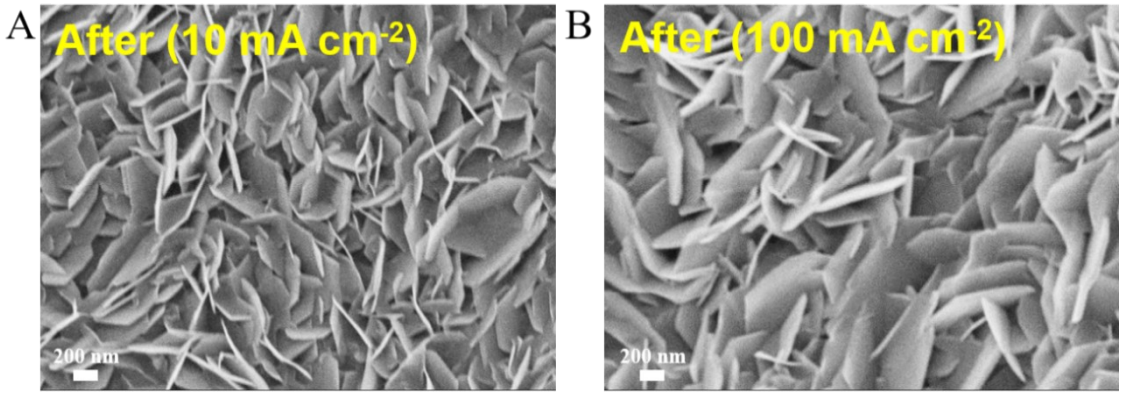

Fig. S5 (A, B) SEM images of Ni_2Fe_1-LDH/rGO/NF after the 24 h HER chronoamperometry measurement.

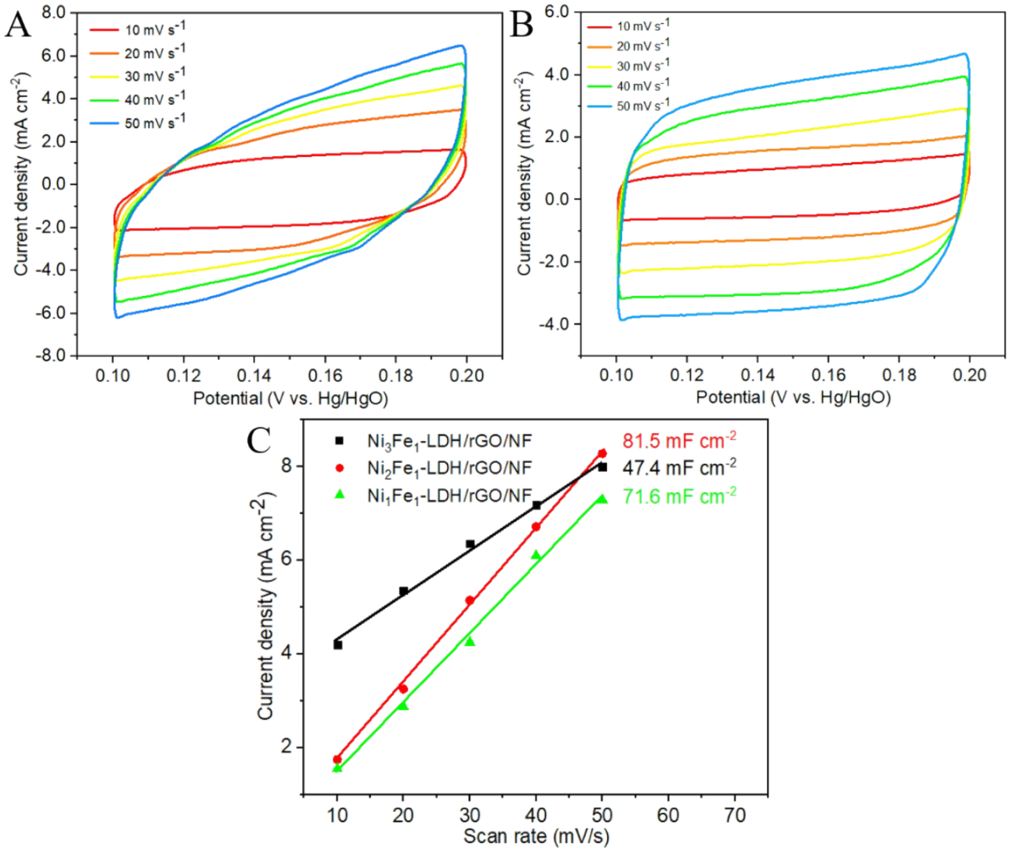

Fig. S6 Cyclic voltammetry curves in the region of 0.2-0.3 V vs Hg/HgO of (A) Ni_3Fe_1-LDH/rGO/NF and (B) Ni_1Fe_1-LDH/rGO/NF at various scan rates. (C) The capacitive current densities of Ni_xFe_1-LDH/rGO/NF (x=3, 2, 1) plotted against different scan rates (10, 20, 30, 40, 50 mV s^{-1}).

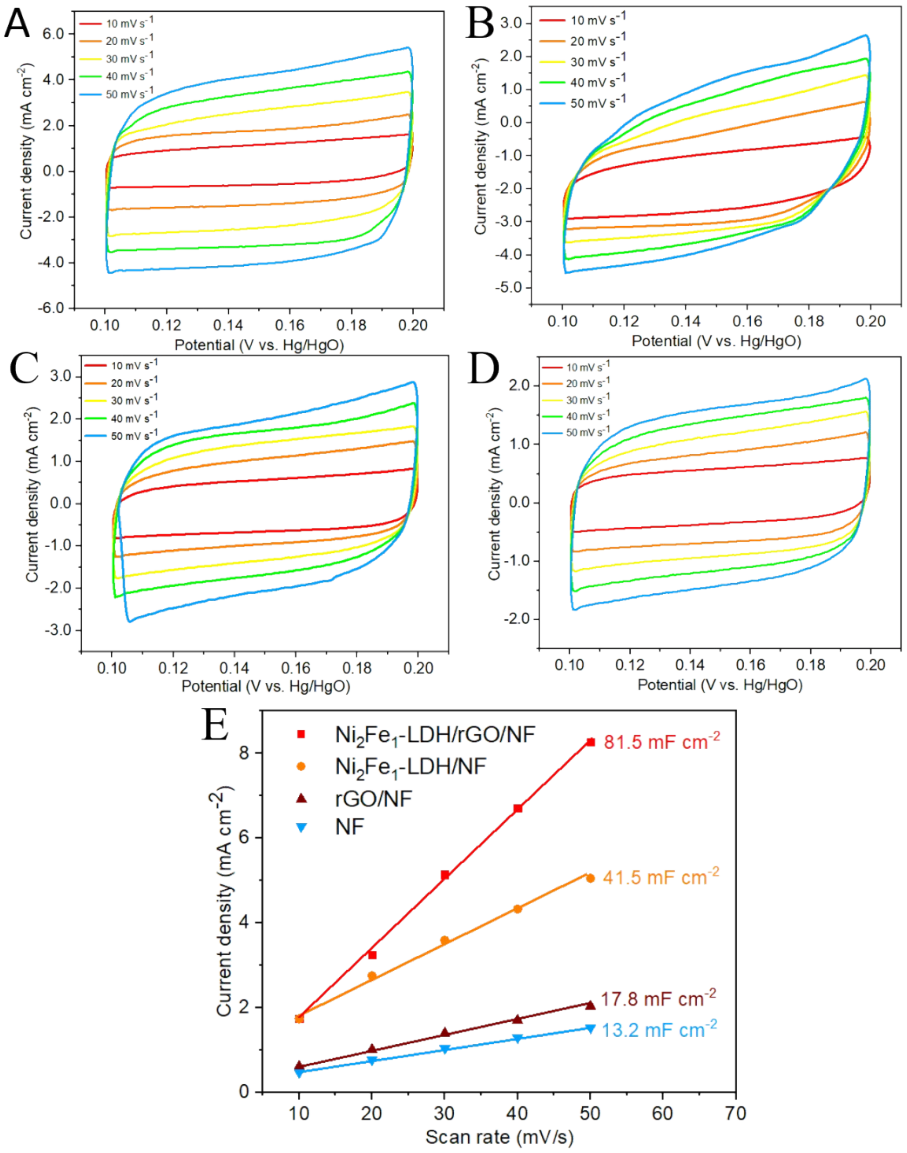

Fig. S7 (A-D) Cyclic voltammetry curves of Ni_2Fe_1-LDH/rGO/NF, Ni_2Fe_1-LDH/NF, rGO/NF and bare NF at various scan rates in the region of 0.2-0.3 V vs Hg/HgO. (E) The capacitive current densities of Ni_2Fe_1-LDH/rGO/NF and control samples Ni_2Fe_1-LDH/NF, rGO/NF and bare NF plotted against different scan rates (10, 20, 30, 40, 50 mV s^{-1}).

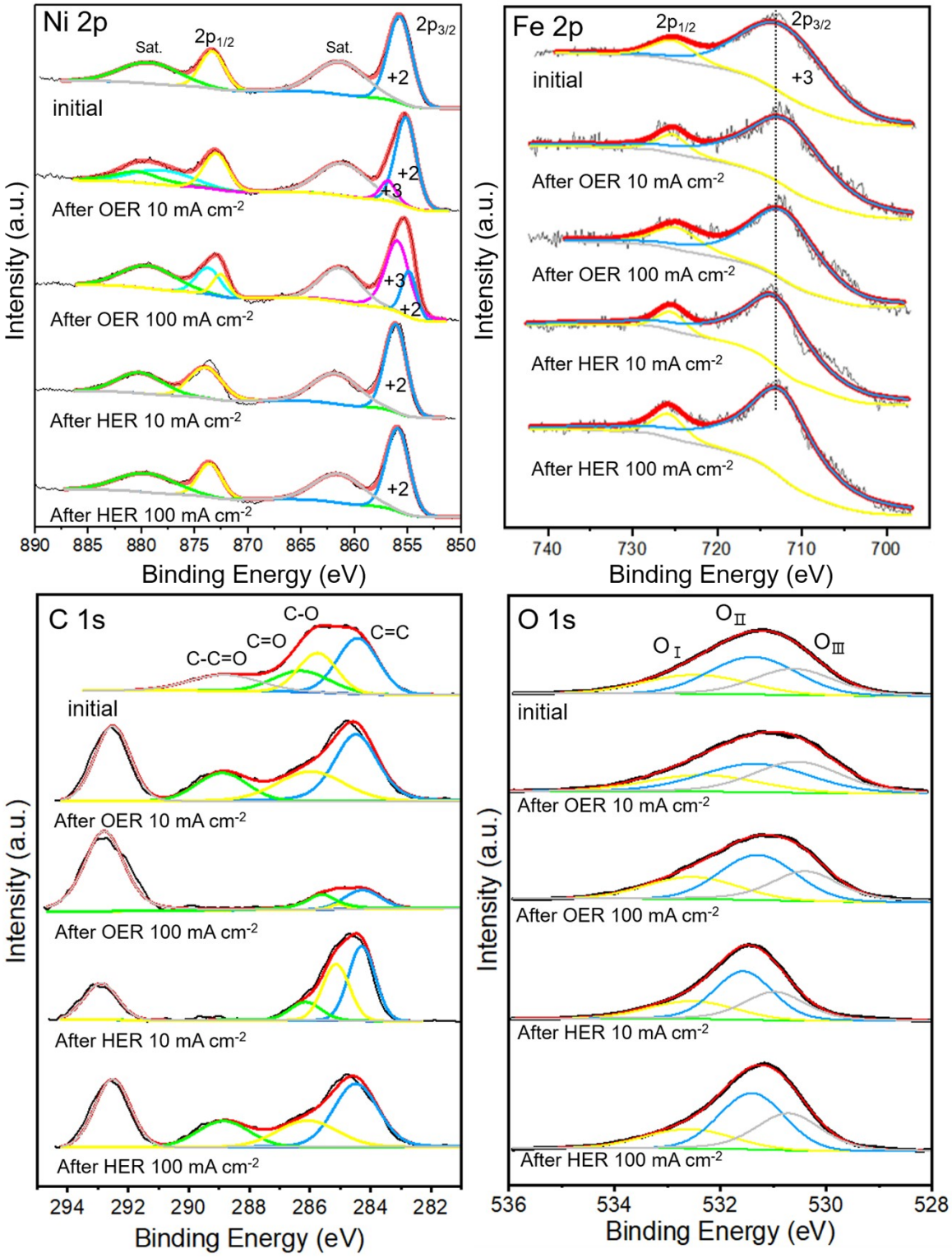

Fig. S8 Ni 2p, Fe 2p, C 1s and O 1s XPS spectrums of Ni_2Fe_1-LDH/rGO/NF before and after the chronoamperometry measurement.

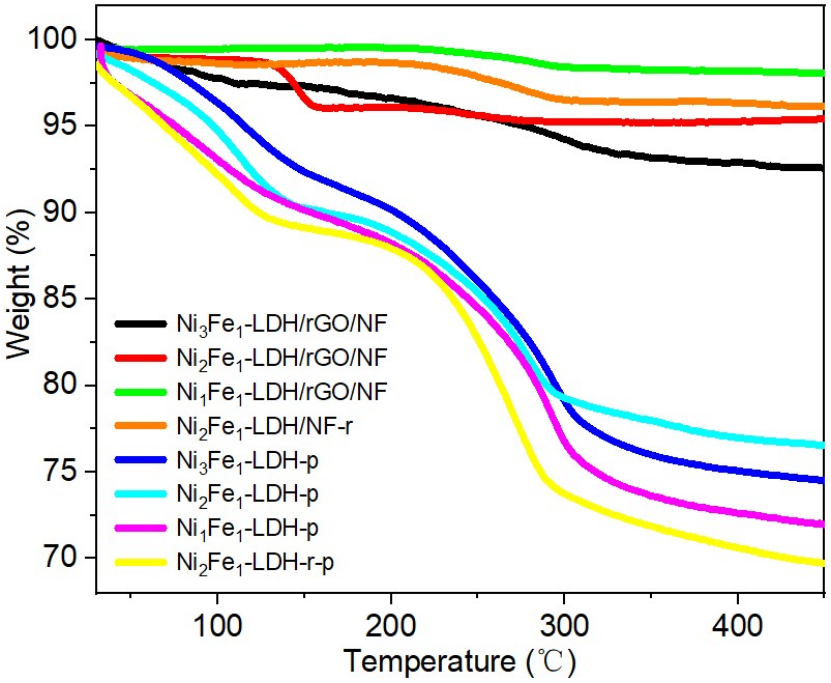

Fig. S9 TGA plots of Ni_xFe_1-LDH/rGO/NF (x=3, 2, 1), Ni_2Fe_1-LDH/NF and the respective LDH. The "r" suffix stands for the reference sample and the "p" suffix stands for the scraped down powder material.

The way to calculate the mass loading: Assuming the mass of Ni_3Fe_1-LDH/rGO/NF is x, and the weight loss ratios of Ni_3Fe_1-LDH/rGO/NF and Ni_3Fe_1-LDH-p are y% and z%, respectively, the loading capacity of Ni_3Fe_1-LDH/rGO/NF is $x \cdot y/z$. The calculation methods of Ni_2Fe_1-LDH/rGO/NF, Ni_1Fe_1-LDH/rGO/NF and Ni_2Fe_1-LDH/NF-r are the same. The mass loading of electrocatalyst on the rGO/NF of Ni_xFe_1-LDH/rGO/NF (x=3, 2, 1) composites and control sample Ni_2Fe_1-LDH/NF are 6.21, 5.19, 5.86 and 4.14 mg cm^{-2}, respectively.

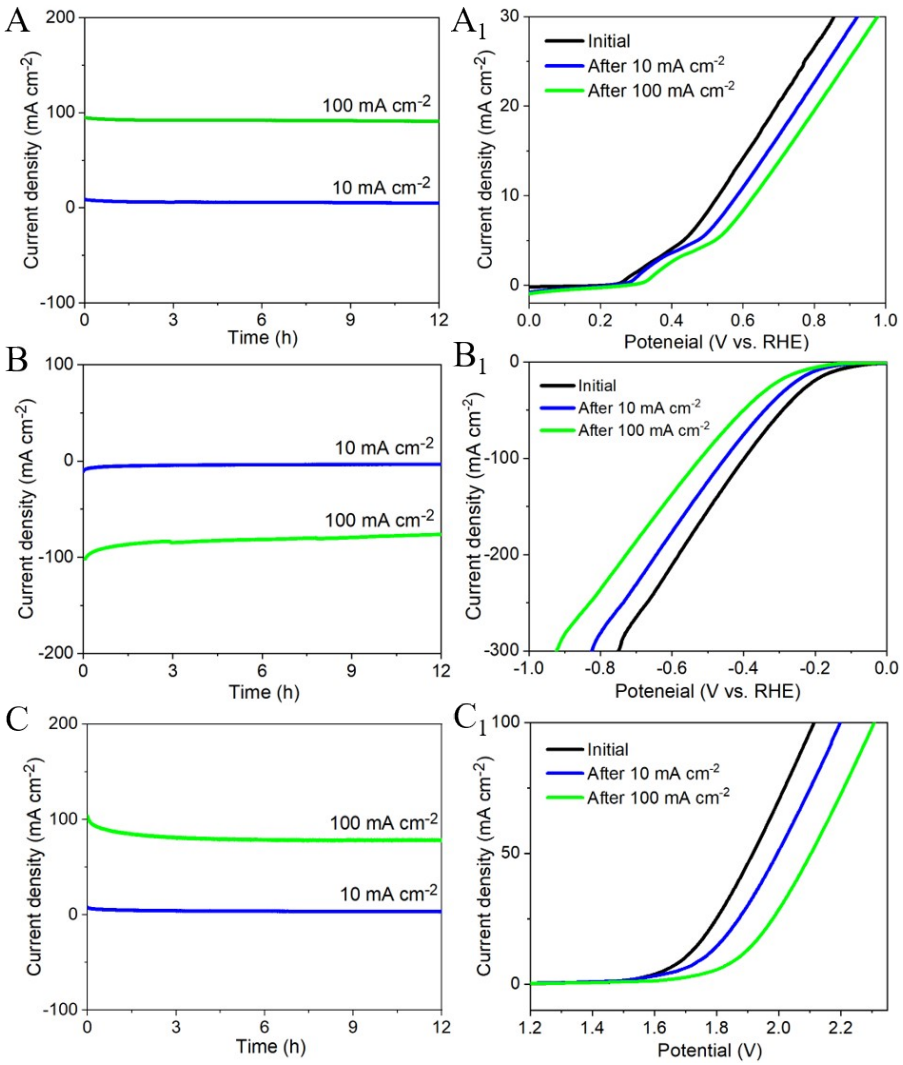

Fig. S10 Chronoamperometry measurements of Ni_2Fe_1-LDH/NF composite for 12 h at 10 and 100 mA cm^{-2} for OER (A), HER (B) and overall water splitting (C) and corresponding performance comparisons before and after the test 1M KOH (A_1, B_1 and C_1).

Table S1 XRD parameters of Ni_xFe_1-LDH/rGO/NF (x=3, 2, 1) composites and control sample Ni_2Fe_1-LDH/NF.

Samples	d_{003}(nm)	d_{110}(nm)	c(nm)[a]	a(nm)[a]	D_{003}(nm)[b]	D_{110}(nm)[b]
Ni_3Fe_1-LDH/rGO/NF	0.7815	0.1550	2.3445	0.3100	10.30	21.63
Ni_2Fe_1-LDH/rGO/NF	0.7859	0.1551	2.3876	0.3101	13.44	24.75
Ni_1Fe_1-LDH/rGO/NF	0.7901	0.1546	2.3702	0.3092	15.31	29.74
Ni_2Fe_1-LDH/NF	0.7929	0.1548	2.3787	0.3095	14.21	24.91

[a] Based on the hexagonal system, $a=2d_{110}$, $c=3d_{003}$;

[b] Based on the Scherer formula $D_{(hkl)}=k\lambda/\beta(\cos\theta)$ ($k=0.89$; λ is the X-ray wavelength, Cu kα: 0.15418 nm; β is the half-height width of the diffraction peak (radians); θ is the Bragg diffraction angle in degree).

Table S2 EIS fitting parameters from equivalent circuits of all electrocatalysts during OER process.

Electrocatalysts	Impedimetric parameters (1M KOH)							
	L (H cm^{-2})	R_s (Ω cm^{-2})	Q-Y_o (S s^n cm^{-2})	Q-n	R_f (Ω cm^{-2})	Q-Y_o (S s^n cm^{-2})	Q-n	R_{ct} (Ω cm^{-2})
Ni_3Fe_1-LDH/rGO/NF	$9.137*10^{-6}$	1.463	0.053	0.216	1.571	0.131	0.832	16.3
Ni_2Fe_1-LDH/rGO/NF	$9.222*10^{-7}$	1.307	0.189	0.531	1.659	0.089	0.512	7.51
Ni_1Fe_1-LDH/rGO/NF	$8.937*10^{-7}$	1.325	0.568	0.713	1.366	0.235	0.463	11.5
Ni_2Fe_1-LDH/NF	$8.723*10^{-6}$	1.899	1.468	0.331	21.53	0.527	0.639	18.5
rGO/NF	$9.453*10^{-6}$	2.264	0.039	0.213	0.311	0.973	0.723	23.1
NF	$9.659*10^{-7}$	2.563	0.431	0.967	2.796	0.032	0.763	26.3

Table S3 Comparison of the electrocatalytic OER activity of Ni_xFe_1-LDH/rGO/NF (x=3, 2, 1) composites with other representative non-noble-metal OER electrocatalysts in basic solution recently reported in the literatures (η10: overpotential at 10 mA cm^{-2}).

Electrocatalyst	Substrate	Method	η_{10} (mV)	Tafel Slope (mV dec^{-1})	Stability (h)	Reference
Ni_3Fe_1-LDH/rGO/NF	Ni foam	hydrothermal	256	55	/	This work
Ni_2Fe_1-LDH/rGO/NF			228	37	24	
Ni_1Fe_1-LDH/rGO/NF			244	47	/	
NiFe-LDH/graphene/Ni foam	Ni foam	CVD, hydrothermal	325	44	2.22	[5]
NiFe-LDH/RGO/NF	Ni foam	chemical reduction, electrodeposition	150	35	10	[6]
NiFe-LDH/rGO@NF	Ni foam	hydrothermal	277@ η_{50}	59.9	24	[7]
NiFe LDH/rGO	glassy carbon	solvothermal	250	33	1.11	[8]
NiFe-LDH/3D-ErGO	Au-RDE	electrodeposition	259	39	2	[9]
NiFe-LDH/NrGO	Ni foam	solvothermal	258	63	9	[10]
0.8 GO-FeNi-LDH	Ni foam	electrodeposition	285	33	25	[11]
NiFe LDH/CNT	glassy carbon	solvothermal	247	31	2	[12]
NiFe LDH–UF	graphite paper	coprecipitation and ultrasonication	254	32	12	[13]
Flower-like Ni-Fe LDH	glassy carbon	hydrothermal	344	97	11	[14]
Exfoliated NiFe NS	glassy carbon	hydrothermal	302	40	12	[15]
NiFeCo LDH/NF	Ni foam	electrodeposition	210	39	50	[16]
$Ni_{2.5}Co_{0.5}Fe$/NF	Ni foam	electrodeposition	275	99	2.8	[17]
NiFeRu LDH/NF	Ni foam	hydrothermal	225	32	10	[18]
Ni_3S_2@NGCLs/NF	Ni foam	CVD	271	99	40	[19]

Table S4 EIS fitting parameters from equivalent circuits of all electrocatalysts during HER process.

Electrocatalysts	Impedimetric parameters (1M KOH)				
	L (H cm^{-2})	R_s (Ω cm^{-2})	Q-Y_o (S s^n cm^{-2})	Q-n	R_{ct} (Ω cm^{-2})
Ni_3Fe_1-LDH/rGO/NF	$7.261*10^{-7}$	1.49	0.0815	0.82	26.8
Ni_2Fe_1-LDH/rGO/NF	$6.662*10^{-8}$	1.52	0.0617	0.80	7.63
Ni_1Fe_1-LDH/rGO/NF	$8.176*10^{-7}$	1.66	0.0352	0.78	16.1
Ni_2Fe_1-LDH/NF	$9.265*10^{-7}$	1.76	0.2943	0.80	37.7
rGO/NF	$9.643*10^{-8}$	1.59	0.0873	0.82	46.7
NF	$9.013*10^{-7}$	1.93	0.1126	0.81	52.9

Table S5 Comparison of the electrocatalytic HER activity of Ni_xFe_1-LDH/rGO/NF (x=3, 2, 1) composites with other representative non-noble-metal HER electrocatalysts in basic solution recently reported in the literatures (η10: overpotential at 10 mA cm^{-2}).

Electrocatalyst	Substrate	Method	η_{10} (mV)	Tafel Slope (mV dec^{-1})	Stability (h)	Reference
Ni_3Fe_1-LDH/rGO/NF	Ni foam	hydrothermal	131	143	/	This work
Ni_2Fe_1-LDH/rGO/NF			109	121	24	
Ni_1Fe_1-LDH/rGO/NF			117	130	/	
0.8 GO-FeNi-LDH	Ni foam	electrodeposition	119	36	25	[11]
NiFe LDH/NF	Ni foam	hydrothermal	210	59	3	[20]
$NiFe_2O_4$/NiFe LDH/NF	Ni foam	hydrothermal	101	67	20	[21]
NiFe LDH/$NiCo_2O_4$/NF	Ni foam	hydrothermal	192	59	10	[22]
NiFe LDH@NiCoP/NF	Ni foam	hydrothermal	120	88	100	[23]
NiFe/$NiCo_2O_4$/NF	Ni foam	hydrothermal	105	39	10	[24]
EG/$Co_{0.85}$Se/NiFe LDH	graphite foil	hydrothermal	260	125	10	[25]
$NiCo_2S_4$@NiFe LDH/NF	Ni foam	hydrothermal	200	101	12	[26]

Table S6 Comparison of O 1s XPS of Ni_2Fe_1-LDH/rGO/NF before and after the chronoamperometry measurement.

Ni_2Fe_1-LDH/rGO/NF	O 1s (eV)		
	O_I	O_{II}	O_{III}
Initial	532.33 (19.23%)	531.22 (44.94%)	530.75 (35.83%)
After OER (10 mA cm^{-2})	532.33 (22.80%)	531.32 (40.22%)	530.54 (36.98%)
After OER (100 mA cm^{-2})	532.52 (25.60%)	531.28 (43.63%)	530.39 (30.77%)
After HER (10 mA cm^{-2})	532.53 (23.04%)	531.56 (46.13%)	530.96 (30.84%)
After HER (100 mA cm^{-2})	532.59 (25.60%)	531.39 (43.63%)	530.70 (30.77%)

Table S7 Comparison of Ni_2Fe_1-LDH/rGO/NF with previously reported bifunctional electrocatalysts for overall water splitting in 1 M KOH.

Electrocatalyst	Method	Substrate	Current density/mA cm^{-2}	Cell voltage	Stability (h)	Reference
Ni_2Fe_1-LDH/rGO/NF	hydrothermal	Ni foam	10	1.62	24	This work
NiCoFeB	chemical reduction	glassy carbon	10	1.81	20	[27]
FeCoNi/NG	annealing	rotating disk	10	1.69	10	[28]
NiFe/$NiCo_2O_4$/NF	hydrothermal, electrodeposition	Ni foam	10	1.67	10	[24]
CoFe/NF	electrodeposition	Ni foam	10	1.64	50	[29]
$Ni_{0.5}Co_{0.5}$/NC film	reactive PLD deposition	NC film	10	1.75	5	[30]
Ni_3Se_2	electrodeposition	Cu foam	10	1.65	12	[31]
Co-P-B-5	chemical reduction	glassy carbon	10	1.65	/	[32]
Mo-Co_9S_8@C	solvothermal	carbon cloth	10	1.68	24	[33]

References

1. X. Xu, H. Chu, Z. Zhang, P. Dong, R. Baines, P. Ajayan, J. Shen and M. Ye, *ACS Appl. Mater. Interfaces*, 2017, **9**, 32756-32766.
2. L. Dou, T. Fan and H. Zhang, *Catal. Sci. Technol.*, 2015, **5**, 5153-5167.
3. L. Dou and H. Zhang, *J. Mater. Chem. A.*, 2016, **4**, 18990-19002.
4. J. Li, Y. Song, Y. Wang and H. Zhang, *ACS Appl. Mater. Interfaces*, 2020, **12**, 50365-50376.
5. H. Wang, C. Tang and Q. Zhang, *J. Mater. Chem. A.*, 2015, **3**, 16183-16189.
6. C. Li, J. Chen, Y. Wu, W. Cao, S. Sang, Q. Wu, H. Liu and K. Liu, *Int. J. Hydrogen Energy*, 2019, **44**, 2656-2663.
7. J. Chen, C. Liu, W. Ren, J. Sun, Y. Zhang and L. Zou, *J. Alloys Compd.*, 2022, **901**, 163510.
8. D. Xia, L. Zhou, S. Qiao, Y. Zhang, D. Tang, J. Liu, H. Huang, Y. Liu and Z. Kang, *Mater. Res. Bull.*, 2016, **74**, 441-446.
9. X. Yu, M. Zhang, W. Yuan and G. Shi, *J. Mater. Chem. A.*, 2015, **3**, 6921-6928.
10. T. Zhan, X. Liu, S. Lu and W. Hou, *Appl. Catal. B: Environ.*, 2017, **205**, 551-558.
11. X. Han, N. Suo, C. Chen, Z. Lin, Z. Dou, X. He and L. Cui, *Int. J. Hydrogen Energy*, 2019, **44**, 29876-29888.
12. M. Gong, Y. Li, H. Wang, Y. Liang, J. Wu, J. Zhou, J. Wang, T. Regier, F. Wei and H. Dai, *J. Am. Chem. Soc.*, 2013, **135**, 8452-8455.
13. Y. Zhao, X. Zhang, X. Jia, G. Waterhouse, R. Shi, X. Zhang, F. Zhan, Y. Tao, L. Wu, C. Tung, D. O'Hare and T. Zhang, *Adv. Energy Mater.*, 2018, **8**, 1703585.
14. L. Zhou, X. Huang, H. Chen, P. Jin, G. Li and X. Zou, *Dalton Trans.*, 2015, **44**, 11592-11600.
15. F. Song and X. Hu, *Nat. Commun.*, 2014, **5**, 4477.
16. P. Babar, A. Lokhande, V. Karade, B. Pawar, M. Gang, S. Pawar and J. Kim, *ACS Sustain. Chem. Eng.*, 2019, **7**, 10035-10043.
17. X. Zhu, C. Tang, H. Wang, B. Li, Q. Zhang, C. Li, C. Yang and F. Wei, *J. Mater. Chem. A.*, 2016, **4**, 7245-7250.
18. G. Chen, T. Wang, J. Zhang, P. Liu, H. Sun, X. Zhuang, M. Chen and X. Feng, *Adv. Mater.*, 2018, **30**, 1706279.
19. B. Li, Z. Li, Q. Pang and J. Zhang, *Chem. Eng. J.*, 2020, **401**, 126045.
20. J. Luo, J. Im, M. Mayer, M. Schreier, M. Nazeeruddin, N. Park, S. Tilley, H. Fan and M. Graetzel, *Science*, 2014, **345**, 1593-1596.
21. Z. Wu, Z. Zou, J. Huang and F. Gao, *ACS Appl. Mater. Interfaces*, 2018, **10**, 26283-26292.
22. Z. Wang, S. Zeng, W. Liu, X. Wang, Q. Li, Z. Zhao and F. Geng, *ACS Appl. Mater. Interfaces*, 2017, **9**, 1488-1495.
23. H. Zhang, X. Li, A. Hähnel, V. Naumann, C. Lin, S. Azimi, S. Schweizer, A. W. Maijenburg and R. Wehrspohn, *Adv. Funct. Mater.*, 2018, **28**, 1706847.

24. C. Xiao, Y. Li, X. Lu and C. Zhao, *Adv. Funct. Mater.*, 2016, **26**, 3515-3523.
25. H. Yang, M. Lohe, Z. Jian, S. Liu and X. Feng, *Energy Environ. Sci.*, 2015, **9**, 478-483.
26. J. Liu, J. Wang, B. Zhang, Y. Ruan, L. Lv, X. Ji, K. Xu, L. Miao and J. Jiang, *ACS Appl. Mater. Interfaces*, 2017, **9**, 15364-15372.
27. Y. Li, B. Huang, Y. Sun, M. Luo, Y. Yang, Y. Qin, L. Wang, C. Li, F. Lv, W. Zhang and S. Guo, *Small*, 2019, **15**, 1804212.
28. Y. Yang, Z. Lin, S. Gao, J. Su, Z. Lun, G. Xia, J. Chen, R. Zhang and Q. Chen, *ACS Catal.*, 2017, **7**, 469-479.
29. P. Babar, A. Lokhande, H. Shin, B. Pawar, M. Gang, S. Pawar and J. Kim, *Small*, 2018, **14**, 1702568.
30. B. Bayatsarmadi, Y. Zheng, V. Russo, L. Ge, C. S. Casari and S.-Z. Qiao, *Nanoscale*, 2016, **8**, 18507-18515.
31. J. Shi, J. Hu, Y. Luo, X. Sun and A. Asiri, *Catal. Sci. Technol.*, 2015, **5**, 4954-4958.
32. A. Chunduri, S. Gupta, O. Bapat, A. Bhide, R. Fernandes, M. K. Patel, V. Bambole, A. Miotello and N. Patel, *Appl. Catal. B: Environ.*, 2019, **259**, 118051.
33. L. Wang, X. Duan, X. Liu, J. Gu, R. Si, Y. Qiu, Y. Qiu, D. Shi, F. Chen, X. Sun, J. Lin and J. Sun, *Adv. Energy Mater.*, 2020, **10**, 1903137.